Proceedings of 20th International Congress on Acoustics, ICA 2010

23-27 August 2010, Sydney, Australia

Evaluation of the effects of secondary radiation Force on aggregation of ultrasound contrast agents

Yanli Zhang, Xiasheng Guo, Dong Zhang, and Xiufen Gong

Institute of Acoustics, Key Laboratory of Modern Acoustics, Ministry of Education, Nanjing University, Nanjing, P.R.China

PACS: 43.25.Yw, 43.35.-c ;

ABSTRACT

Ultrasound contrast agents have show promising for ultrasonic molecular imaging, in which targeted agents selectively attach molecular markers expressed on diseased endothelium and increase contrast in the area such as thrombus and inflammation. Ultrasound radiation force can manipulate encapsulated microbubbles and displace them off the vessel axis in blood stream towards the vessel wall, thus increase the targeting efficiency in ultrasonic molecular imaging. However, the secondary radiation force produces a reversible attraction and aggregation of microbubbles, limiting the improvement of imaging sensitivity. This study proposed a theoretical model of second radiation force for encapsulated microubbles. In this theoretical model, the nonlinear radial oscillations of microbubbles are described by a modfied Herring equation including the change of the suface tension during oscillation, and coupled with the translation motions of microbubbles. This model is then used in a numerical investigation of the translational motion of encapsulated microbubbles in ultrasound molecular imaging. Results indicate that the secondary radiation force provides a significant effect on the aggregation of microbubbles, and its effect is associated with the ultrasound frequency, amplitude, and microbubble concentration. The results obtained are of interest for developing a high sensitive technique for detection of adhesive microbubbles from free microbubbles.

INTRODUCTION

In the targeted imaging system, microbubbles are used as targeted contrast agents, which are expected to adhere to a specific site with a binding mechanism [1]. Ultrasound radiation force was proposed to drive microbubbles for increasing the binding efficiency [2, 3]. However, these studies are based on the assumption of no interaction between microbubbles. As distance of only a few microns between bubbles is common in ultrasound molecular imaging, the short-range secondary radiation force may produce an aggregate of bubbles4. As a result, the formation of aggregation has a negative effect on their circulation in the blood flow, and even leading to wrong target in clinical applications.

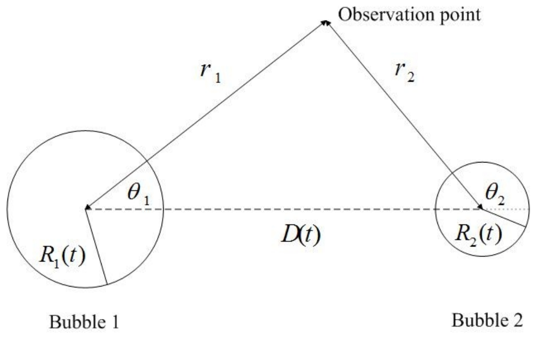

Figure 1. Schematic diagram for two pulsating and translating bubbles.

The purpose of this study is to evaluate the effects of secondary radiation force on aggregation of ultrasound contrast agents. We first calculate the dynamic interaction of a binary bubble system and find that the mutual forces appear as attraction for bubble pairs in the 0.8 to 3μm radius size we are interested in. And then, for such bubbles, the influence of different driving amplitudes, frequencies, distance between centers of the two, and shell parameters on the degree of aggregation between them is numerically investigated.

THEORETICAL MODEL

Consider that two coated microbubbles with radii R_{10} and R_{20} in an incompressible viscous liquid exposed to an acoustic wave field. Both microbubbles undergo volume and translational oscillations. Let $R_1(t)$ and $R_2(t)$ denote the time-dependent microbubble radii, and $D(t)$ the time-dependent distance between the bubble centers. As shown in Figure 1, local axisymmetric spherical coordinates originated at and translated with the centers of the microbubbles are used. In a previous study [5], equations of radial and translational oscillations of two interacting spherical gas bubbles in an incompressible liquid are given by

$$R_1\ddot{R}_1+\frac{3}{2}\dot{R}_1^2-\frac{p_1}{\rho}=\frac{\dot{x}_1^2}{4}-\frac{R_2^2\ddot{R}_2+2R_2\dot{R}_2^2}{D}+\frac{R_2^2(\dot{x}_1\dot{R}_2+R_2\ddot{x}_2+5\dot{R}_2\dot{x}_2)}{2D^2}-\frac{R_2^3\dot{x}_2(\dot{x}_1+2\dot{x}_2)}{2D^3} \qquad (1)$$

$$R_2\ddot{R}_2+\frac{3}{2}\dot{R}_2^2-\frac{p_2}{r}=\frac{\dot{x}_2^2}{4}-\frac{R_1^2\ddot{R}_1+2R_1\dot{R}_1^2}{D}-\frac{R_1^2(\dot{x}_2\dot{R}_1+R_1\ddot{x}_1+5\dot{R}_1\dot{x}_1)}{2D^2}-\frac{R_1^3\dot{x}_1(\dot{x}_2+2\dot{x}_1)}{2D^3} \quad (2)$$

$$\frac{R_1\ddot{x}_1}{3}+\dot{R}_1\dot{x}_1+\frac{1}{D^2}\frac{d}{dt}(R_1R_2^2\dot{R}_2)-\frac{R_2^2(R_1R_2\ddot{x}_2+R_2\dot{R}_1\dot{x}_2+5R_1\dot{R}_2\dot{x}_2)}{D^3}=\frac{F_{ex1}}{2prR_1^2} \quad (3)$$

$$\frac{R_2\ddot{x}_2}{3}+\dot{R}_2\dot{x}_2-\frac{1}{D^2}\frac{d}{dt}(R_2R_1^2\dot{R}_1)-\frac{R_1^2(R_1R_2\ddot{x}_1+R_1\dot{R}_2\dot{x}_1+5R_2\dot{R}_1\dot{x}_1)}{D^3}=\frac{F_{ex2}}{2prR_2^2} \quad (4)$$

which allows for the radiation coupling between the bubbles with accuracy up to third order in the inverse separation distance $D(t)$. Eqs. (1) and (2) govern the volume pulsation of the jth bubble and Eqs. (3) and (4) their translational motion. Here $R_j(t)$ and $x_j(t)$ denote the time-varying radii and position of the center of the jth (j=1, 2) bubble, respectively. p_j is the scattered pressure at the surface of the jth bubble, F_{exj} is an external force on the jth bubble such as viscous drag, and the overdot denotes the time derivative d/dt.

The dynamics of encapsulated bubbles are affected by both of its shell and the gas core. To consider the effects of the shell, two additional terms are included. The first term introduces an effective surface tension of the shell following the model of Marmottant *et al.* [6] $s(R)\approx s(R_0)+2c(R/R_0-1)$ at elastic state. And c is the elastic modulus of the shell. The second is a damping term due to the viscosity of the shell, which is given by $12m_{sh}e\dot{R}/[R(R-e)]$ [7]. Here m_{sh} is the viscosity of the shell material and e is the shell thickness. To allow for these factors, the left-hand side of Eqs. (1) and (2), which are the well-known Rayleigh-Plesset equation, are replaced by the modified Herring equation [3] to give

$$R_1\ddot{R}_1+\frac{3}{2}\dot{R}_1^2-\frac{1}{r}\left(P_1+\frac{R_1}{c}\dot{P}_1-P_0-P_{driv}\right)=\frac{\dot{x}_1^2}{4}-\frac{R_2^2\ddot{R}_2+2R_2\dot{R}_2^2}{D}+\frac{R_2^2(\dot{x}_1\dot{R}_2+R_2\ddot{x}_2+5\dot{R}_2\dot{x}_2)}{2D^2}-\frac{R_2^3\dot{x}_2(\dot{x}_1+2\dot{x}_2)}{2D^3} \quad (5)$$

$$R_2\ddot{R}_2+\frac{3}{2}\dot{R}_2^2-\frac{1}{r}\left(P_2+\frac{R_2}{c}\dot{P}_2-P_0-P_{driv}\right)=\frac{\dot{x}_2^2}{4}-\frac{R_1^2\ddot{R}_1+2R_1\dot{R}_1^2}{D}-\frac{R_1^2(\dot{x}_2\dot{R}_1+R_1\ddot{x}_1+5\dot{R}_1\dot{x}_1)}{2D^2}-\frac{R_1^3\dot{x}_1(\dot{x}_2+2\dot{x}_1)}{2D^3} \quad (6)$$

here,

$$P_j=\left(P_0+\frac{2s_0}{R_0}\right)\left(\frac{R_0}{R_j}\right)^{3g}-\frac{4m\dot{R}_j}{R_j}-\frac{2s_0}{R_j}-4c\left(\frac{1}{R_0}-\frac{1}{R_j}\right)-12m_{sh}e\,\frac{\dot{R}_j}{R_j(R_j-e)} \quad (7)$$

Where P_j is the pressure in the liquid at the bubble wall, $P_{driv}(t)$ is the driving acoustic pressure field which we assume as $P_{driv}(t)=-P_a\sin(2pft)$, s_0 is the equilibrium surface tension, g is the polytrophic gas exponent, and m is the viscosity of the liquid. The external forces F_{exj} are taken in the form [5],

$$F_{exj}=-12pmR_j(\dot{x}_j-v_{3-j}) \quad (8)$$

here

$$v_j=-\frac{(-1)^jR_j^2\dot{R}_j}{D^2}+\frac{R_j^3\dot{x}_j}{D^3} \quad (9)$$

RESULTS AND DISCUSSIONS

The values of microbubble parameters in the numerical calculation are given in Table I. Equations (3)-(6) are numerically solved with initial values R_1=R_{10}, R_2=R_{20}, x_1=0, x_2=D_0, R_1=R_2=x_1=x_2 at t=0.

Table 1. Values of microbubble parameters in the numerical calculation.

Symbols	Description	Value
P_0	Hydrostatic pressure (Pa)	1.01×10^5
r	liquid density (kg/m^3)	998
c	Acoustic velocity in liquid (m/s)	1500
s_0	equilibrium surface tension (N/m)	0.051
g	polytrophic gas exponent	1.07
m	viscosity of the liquid (Pa·s)	0.001
c	elastic modulus of the shell (N/m)	≤1
m_{sh}	viscosity of the shell material (Pa·s)	1.27
e	shell thickness (m)	2×10^{-9}

The secondary Bjerknes force coefficient f_B is used to determine the dynamic behavior of two bubbles, which is defined as [8],

$$f_B=\frac{r}{4p}\left\langle\dot{V}_1\dot{V}_2\right\rangle \quad (10)$$

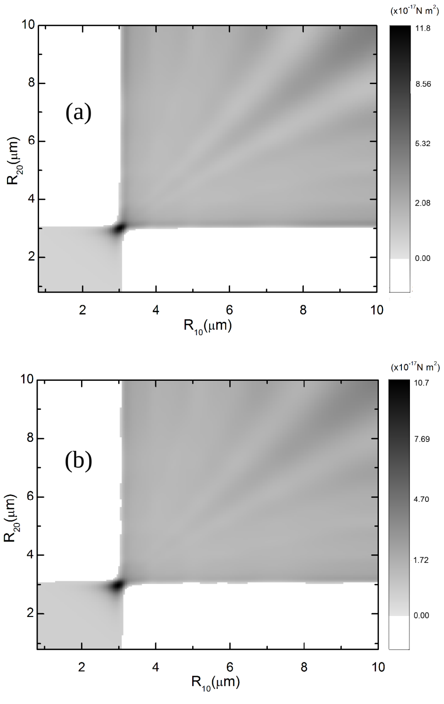

Figure 2. Dynamic behavior of two bubbles (driving amplitude:01MPa, frequency: 2.25 MHz), (a) D_0=120 μm, and (b) D_0=50 μm.

where V_j denotes the volume of the jth bubble. The sign of f_B indicates attraction (f_B>0) or repulsion (f_B<0) of the microbubbles. Numerical calculations were carried out with driving acoustic pressure amplitude P_a=0.1 MPa, and frequency f=2.25 MHz for different initial inter-bubble distances D_0. The resonance radius corresponding to the driving frequency of microbubbles is approximately 2.9 μm. Figure 2 presents the Bjerknes force coefficients in a grayscale mode in the R_{10}-R_{20} plane for the cases with D_0=120 μm and 50 μm, respectively. As can be seen, the analysis predicts the existence of two distinct dynamical regimes. The white areas indicate repulsion, and darker regions attraction. Repulsive region contains bubbles with one smaller and the other larger than the nonlinear resonance size. While the attractive forces prevail as bubbles both have radii larger or smaller than the resonance radius and strongest attractive area locates at resonance radii. When D_0 decreases, the repulsive regions expand to larger sizes. This indicates the inversion of the interaction force and the possibility of the formation of stable bubble pairs in the vicinity of regions corresponding to linear resonance.Type equations from the left margin, with one blank line above and one below to separate them from text. Number equations consecutively with the number in brackets justified on the right hand margin. Symbols should be defined when they are first used.

Figure 3 shows the evolution of secondary Bjerknes force coefficient f_B with a short time frame for a selected bubble pair R_{10}=3 μm and R_{20}=6 μm near resonant regions in Figure 2. An inversion of mutual bubble force can be found as the bubbles come close to each other. For D_0=120 μm, the time averaging yields a positive net f_B drawn from the curve of significantly oscillatory section, and thus bubbles are attracting each other corresponding to the dark region of Figure 2(a). When the bubbles approach to a distance D_0=50 μm, a negative net f_B is observed corresponding to the white region of Figure 2(b). This shows that the interaction force can change from attraction to repulsion as the bubbles approach each other.

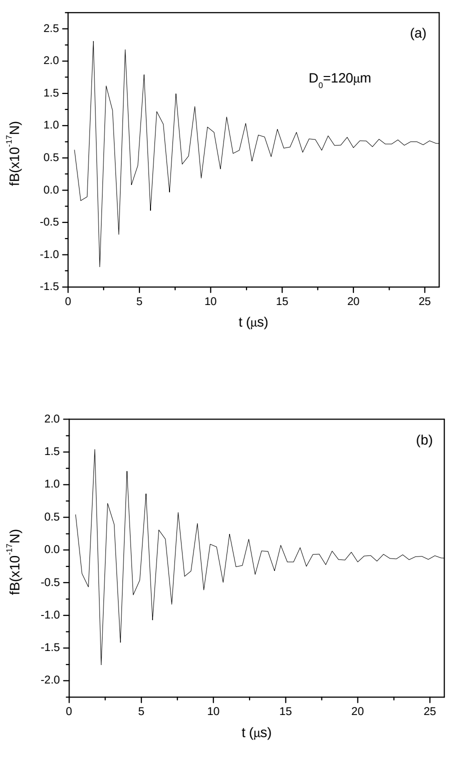

Figure 3. The time-dependent secondary Bjerknes force coefficient f_B of the selected bubble pairs R_{10}=3 μm and R_{20}=6 μm: (a) D_0=120 μm, (b) D_0=50 μm.

The formation of stable bubble pairs is another important aspect of the dynamic behavior of two bubble systems. Figure 4 shows the evolution the average distance between the centers of the two bubbles in the following two situations: (1) the two bubbles attract each other until stable bubble pairs are formed (Figure 4(a)); (2) the two bubbles repel each other until a stable pair is formed (Figure 4(b)). It should be noted that in Figure 4(b) it takes longer time for viscosity to decelerate their motion and produce a steady drift velocity. Accordingly, as time increases the slower moving bubble pair can become a candidate for the formation of stable pairs. Finally the two pairs of interacting bubbles move along the same direction with the same translational velocity , respectively. This seems contrary to the fact that the Bjerknes forces between the two bubbles are the same in magnitude and opposite in sign. However, the viscous drag forces between bubbles of different sizes are not equal in magnitude, thus the effect with movement in the same direction is allowed.

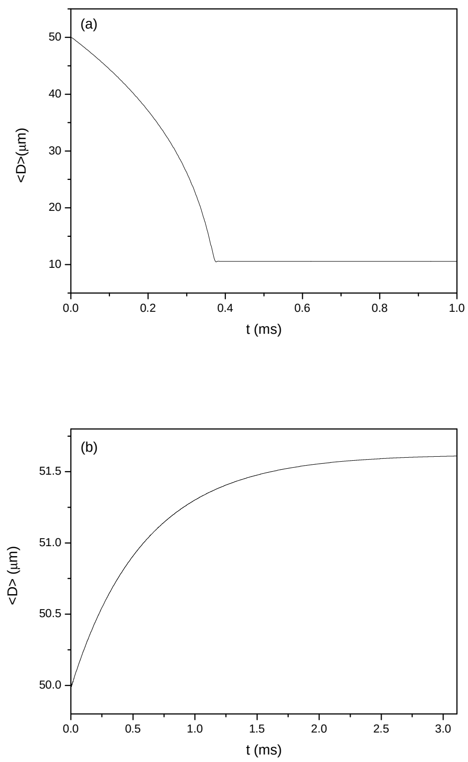

Figure 4. Evolution of the average distance between the centers of the two bubbles with elapsed time: (a) R_{10}=4 μm and R_{20}=6 μm (b) R_{10}=3 μm and R_{20}=6 μm; D_0=50 μm.

CONCLUSIONS

One of major challenges remaining in ultrasonic molecular imaging is the poor targeting efficiency of contrast agents. The influence of the secondary radiation force on aggregation between two small coated bubbles has been investigated in this study. Numerical calculations have been performed based on the modified RP equation and four simultaneous differential equations of radial and translational motion. The change of secondary radiation force signs and the formation of stable bubble pairs in the vicinity of regions corresponding to linear resonance are two important aspects of the dynamic behaviors of two bubble systems. Considering contrast agents used for ultrasound molecular imaging with a radii size on the order of 0.8 to 3 μm, attraction between bubbles readily occurs in clinical practice, resulting in aggregation of agents.

ACKNOWLEDGEMENTS

This work is supported by the National Basic Research Program 973 (Grant No. 2010CB732600) from Ministry of Science and Technology, China, the National Natural Science Foundation of China (10774071 and 10974093) and the State Key Laboratory of Acoustics.

REFERENCES

1. Klibanov, M. Hughes, J. Marsh, C. Hall, J. Miller, J. Wible, and G. Brandenburger, "Targeting of ultrasound contrast material: An in vitro feasibility study," Acta Radiol Suppl. 412,113-120 (1997).
2. S. Zhao, M. Borden, S. H. Bloch, D. Kruse, K. W. Ferrara, and P. A. Dayton, "Radiation-force assisted targeting facilitates ultrasonic molecular imaging," Mol Imaging 3, 135-148 (2004).
3. Y. Hu, D. Zhang, "Chirp excitation technique to enhance microbubble displacement induced by ultrasound radiation force", J. Acoust. Soc. Am. 125, 1410–1415 (2009).
4. P. A. Dayton, K. E. Morgan, A. L. Klibanov, G. H. Brandenburger and K. W. Ferrara, "Optical and Acoustical Observations of the Effects of Ultrasound on Contrasts Agents," IEEE Trans. Ultrason. Ferroelectr. Freq. Control 46, 220-232 (1999).
5. A. Doinikov, ‘‘Translational motion of two interacting bubbles in a strong acoustic field,’’ Phys. Rev. E 64, 026301(2001).
6. P. Marmottant, S. van der Meer, M. Emmer, and M. Versluis, ‘‘A model for large amplitude oscillations of coated bubbles accounting for buckling and rupture," J. Acoust. Soc. Am. 118, 3499–3505 (2005).
7. K. E. Morgan, J. S. Allen, P. A. Dayton, J. E. Chomas, A. L. Klibanov, and K. W. Ferrara, ‘‘Experimental and Theoretical Evaluation of Microbubble Behavior: Effect of TransmittedPhase and Bubble Size", IEEE Trans. Ultrason. Ferroelectr. Freq. Control 47, 1494-1509 (2000).
8. R. Mettin, I. Akhatov, U. Parlitz, CD. Ohl, and W. Lauterborn, ‘‘Bjerknes forces between small cavitation bubbles in a strong acoustic field,’’ Phys. Rev. E 56, 2924–2931 (1997).